

Heterogeneous Photon Recycling and Charge Diffusion Enhance Charge Transport in Quasi-2D Lead-Halide Perovskite Films

Silvia Motti, Timothy Crothers, Rong Yang, Yu Cao, Renzhi Li, Michael B. Johnston, Jianpu Wang, and Laura M. Herz

Nano Lett., **Just Accepted Manuscript** • DOI: 10.1021/acs.nanolett.9b01242 • Publication Date (Web): 09 May 2019

Downloaded from <http://pubs.acs.org> on May 12, 2019

Just Accepted

“Just Accepted” manuscripts have been peer-reviewed and accepted for publication. They are posted online prior to technical editing, formatting for publication and author proofing. The American Chemical Society provides “Just Accepted” as a service to the research community to expedite the dissemination of scientific material as soon as possible after acceptance. “Just Accepted” manuscripts appear in full in PDF format accompanied by an HTML abstract. “Just Accepted” manuscripts have been fully peer reviewed, but should not be considered the official version of record. They are citable by the Digital Object Identifier (DOI®). “Just Accepted” is an optional service offered to authors. Therefore, the “Just Accepted” Web site may not include all articles that will be published in the journal. After a manuscript is technically edited and formatted, it will be removed from the “Just Accepted” Web site and published as an ASAP article. Note that technical editing may introduce minor changes to the manuscript text and/or graphics which could affect content, and all legal disclaimers and ethical guidelines that apply to the journal pertain. ACS cannot be held responsible for errors or consequences arising from the use of information contained in these “Just Accepted” manuscripts.



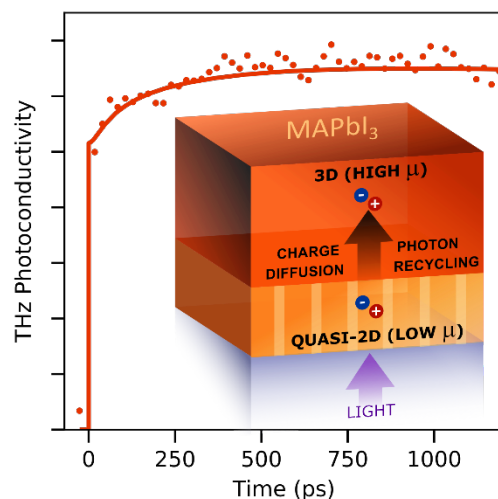
Heterogeneous Photon Recycling and Charge Diffusion Enhance Charge Transport in Quasi-2D Lead-Halide Perovskite Films

Silvia G. Motti,¹ Timothy Crothers,¹ Rong Yang,² Yu Cao,² Renzhi Li,² Michael B. Johnston,¹
Jianpu Wang,^{2#} Laura M. Herz^{1*}

¹ Clarendon Laboratory, Department of Physics, University of Oxford, OX1 3PU, Oxford,
UK

² Key Laboratory of Flexible Electronics (KLOFE) & Institute of Advanced Materials
(IAM), Jiangsu National Synergetic Innovation Center for Advanced Materials (SICAM),
Nanjing Tech University, 30 South Puzhu Road, Nanjing 211816, China

#iamjpwang@njtech.edu.cn, *laura.herz@physics.ox.ac.uk



1
2
3 *The addition of large hydrophobic cations to lead halide perovskites has significantly enhanced*
4 *the environmental stability of photovoltaic cells based on these materials. However, the*
5 *associated formation of two-dimensional structures inside the material can lead to dielectric*
6 *confinement, higher exciton binding energies, wider bandgaps and limited charge-carrier*
7 *mobilities. Here we show that such effects are not detrimental to the charge transport, for*
8 *carefully processed films comprising a self-assembled thin layer of quasi-2D perovskite*
9 *interfaced with a 3D MAPbI₃ perovskite layer. We apply a combination of time-resolved*
10 *photoluminescence and photoconductivity spectroscopy to reveal the charge-carrier*
11 *recombination and transport through the film profile, when either the quasi-2D or the 3D layers*
12 *are selectively excited. Through modelling of the recorded dynamics, we demonstrate that while*
13 *the charge-carrier mobility is lower within the quasi-2D region, charge-carrier diffusion to the*
14 *3D phase leads to a rapid recovery in photoconductivity even when the quasi-2D region is*
15 *initially photoexcited. In addition, the blue-shifted emission originating from quasi-2D regions*
16 *overlaps significantly with the absorption spectrum of the 3D perovskite, allowing for highly*
17 *effective “heterogeneous photon recycling”. We show that this combination fully compensates*
18 *for the adverse effects of electronic confinement, yielding quasi-2D perovskites with highly*
19 *efficient charge transporting properties.*
20
21
22
23
24
25
26
27
28
29
30
31
32
33
34
35
36
37
38
39
40
41
42

43 *Keywords: solar cells, charge-carrier dynamics, mobility, hybrid perovskites, photon*
44 *reabsorption, nanostructured*
45
46
47
48
49
50
51
52
53
54
55
56
57
58
59
60

1
2
3 Metal halide perovskite semiconductors have recently emerged as promising materials for
4 photovoltaic devices, whose efficiencies have reached over 23%.¹ However, a significant
5 obstacle to commercial application is the poor stability of this class of materials, in particular
6 upon exposure to moisture.²⁻⁴ One strategy to overcome this challenge is the addition of large
7 hydrophobic organic cations to the perovskite precursors as part of the film fabrication process,
8 which has proven to enhance the moisture resistance and the environmental stability of the
9 material.^{5,6} Since these molecules are too large to fit into the perovskite octahedra, they instead
10 form interlayers that induce the formation of a two-dimensional (2D) structure. While these
11 hydrophobic spacers thus reduce moisture permeability, they also form a dielectric barrier
12 between adjacent layers of the metal halide perovskite. Such dielectric confinement may result in
13 higher exciton binding energies, wider bandgap and limited charge-carrier diffusion lengths,^{7,8}
14 which are unfavorable characteristics for photovoltaic applications.
15
16
17
18
19
20
21
22
23
24
25
26
27
28
29
30
31
32
33

34 To mitigate the adverse effects of charge confinement upon the addition of hydrophobic
35 molecules, quasi-2D compositions have been fabricated for which the ratio between the small
36 cation incorporated into the perovskite lattice, and the large hydrophobic cation is carefully
37 tuned. Depending on the exact processing conditions, the resulting films contain various
38 distributions of n semiconducting perovskite layers, and consequently different levels of
39 electronic confinement. In addition, hydrophobic interlayers may be placed in a random or
40 gradient (low to high n) arrangement across the film depth. Such mixed-phase materials can
41 combine the enhanced stability of 2D perovskites with the superior charge-transport properties of
42 their 3D counterpart, as has been demonstrated by their successful implementation in light
43 emitting diodes⁹⁻¹² and photovoltaic devices.¹³⁻²⁰
44
45
46
47
48
49
50
51
52
53
54
55
56
57
58
59
60

1
2
3
4
5
6 Many fundamental and practical questions arise from the presence of such chemical and
7
8 electronic heterogeneity inside these mixed-phase perovskites. For instance, it has recently been
9
10 explored how the nature of charge-carriers and their interaction with the lattice differ from what
11
12 is encountered in the more conventional bulk 3D perovskite semiconductors.^{7,8,21-23} For the
13
14 optimized operation of electronics devices, knowledge of how energy and charge transfer occur
15
16 between different domains within mixed-phase materials is particularly important. Although a
17
18 few studies have investigated electronic interactions between neighboring perovskite sheets and
19
20 short-scale transfer mechanisms,²⁴⁻²⁶ an understanding of how these heterogeneities affect charge
21
22 transport throughout a film's depth is urgently required for optimization of charge conduction on
23
24 the device scale.
25
26
27
28
29
30
31
32

33 In this study, we address this issue by investigating mixed-phase quasi-2D/3D lead-iodide
34
35 perovskite films using a combination of time-resolved photoluminescence (PL) and optical-pump
36
37 terahertz-probe (OPTP) spectroscopy. We demonstrate that for the deployed processing
38
39 conditions, the film contains a layer of quasi-2D domains on the side interfacing the substrate,
40
41 and a predominantly 3D region near the outer side of the film. We find that the mobility of
42
43 charge-carriers inside the quasi-2D region is on average ~25% lower than for those present in the
44
45 3D (bulk) layer of the film. However, this seemingly detrimental effect of low dimensionality
46
47 appears to be short-lived, as the OPTP dynamics reveal a transient enhancement of
48
49 photoconductivity over a timescale of ~1 ns after primarily the quasi-2D region is photoexcited.
50
51 By modelling the charge-carrier dynamics in these films, we demonstrate that this
52
53 photoconductivity boost results from charge-carriers transferring efficiently from quasi-2D
54
55
56
57
58
59
60

1
2
3 regions to 3D layers, where the charge mobility is higher. We show that such transfers are not
4
5 only aided by charge-carrier diffusion, but also by photon recycling of higher-energy photons
6
7 emitted from the quasi-2D domains that are particularly efficiently recaptured by the absorption
8
9 profile of the 3D bulk phase. Our findings therefore reveal that the presence of dielectric
10
11 confinement in such mixed phase films may be far less detrimental to photovoltaic performance
12
13 than is commonly assumed. In particular, charge-carrier transfer from quasi-2D to 3D domains
14
15 with higher mobility can be sufficiently rapid to outcompete recombination and is aided by the
16
17 up-shift in emission energy resulting from electronic confinement, which yields particularly
18
19 effective photon reabsorption by the 3D region. Hence, we find that for suitable film morphology
20
21 the enhanced stability of 2D perovskites can be combined with the favorable charge-transport
22
23 properties of 3D semiconductors.
24
25
26
27
28
29
30
31

32 Mixed phase quasi-2D/3D lead iodide perovskite thin films were fabricated on quartz
33
34 substrates, based on the smaller methylammonium (MA) cation for incorporation into the lead
35
36 iodide perovskite lattice, and the larger 3-bromobenzylammonium cation as a spacer (3BBA).
37
38 Full details of the film fabrication and characterization are provided in the SI. A similar film
39
40 fabrication method has recently been successfully applied to yield active layers for efficient solar
41
42 cells with a peak power conversion efficiency of 18.2% and excellent stability in moist
43
44 environment.⁶ The morphology of the films can be examined in Figure 1.a, which shows the
45
46 cross-section of the perovskite film recorded through aberration-corrected scanning transmission
47
48 electron microscope (STEM). While the top surface of the film appears homogeneous, on the
49
50 substrate side, elongated crystallites can be identified which are oriented perpendicular to the
51
52 substrate. Grazing-incidence wide-angle X-ray scattering (GIWAXS) measurements previously
53
54
55
56
57
58
59
60

1
2
3 performed on these films⁶ have revealed that the outer surface is constituted mostly by 3D
4
5 MAPbI₃ crystallites, while additional peaks associated with 2D-phase perovskite could be
6
7 observed for higher incidence angle (when the full depth of the films was being probed).
8
9
10 Moreover, these measurements indicated a predominant orientation of the layered structures
11
12 within the quasi-2D phase perpendicular to the substrate. Previous reports suggest that such
13
14 preferential formation of quasi-2D domains on the substrate side may be linked to specific
15
16 parameters such as the solubility of the precursors, the substrate temperature and surface
17
18 energies.^{7,9-11} Based on our experimental evidence, we conclude that the present mixed-phase films
19
20 comprise two distinct regions, as depicted schematically in Figure 1.b. The top layer on the outer
21
22 surface consists of large 3D MAPbI₃ crystallites while the substrate-side layer constitutes a blend
23
24 of smaller 3D crystallites and quasi-2D domains, whose preferential orientation is perpendicular
25
26 to the film surface.
27
28
29
30
31
32
33
34
35
36
37
38
39
40
41
42
43
44
45
46
47
48
49
50
51
52
53
54
55
56
57
58
59
60

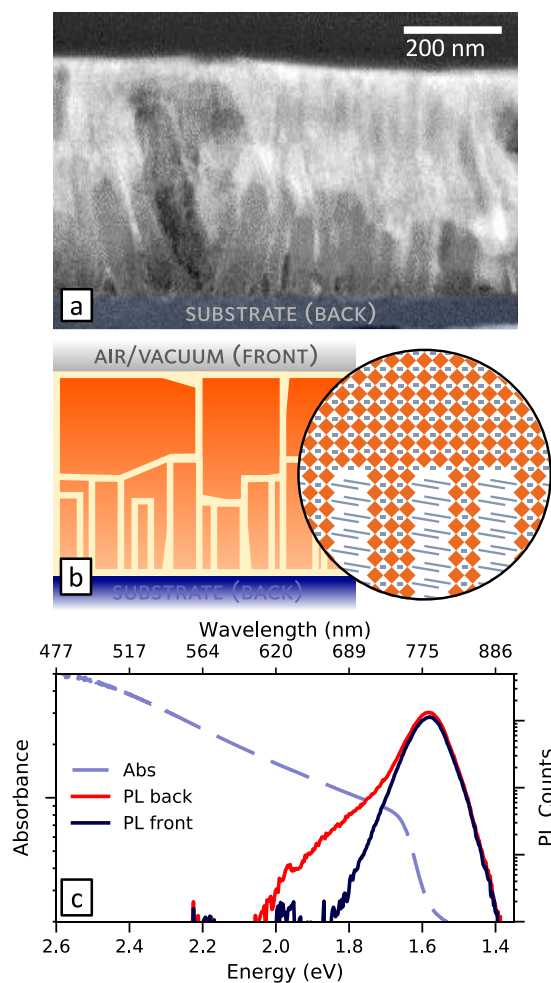


Figure 1. a) Cross-section of the lead iodide perovskite film recorded by scanning transmission electron microscope (STEM); b) Schematic illustration of the film morphology, showing 3D MAPbI₃ crystallites on top and orientated quasi-2D crystallites at the substrate side; c) Absorption (dashed line, light blue) and PL spectra taken in reflection geometry with excitation at 3.1 eV photon energy, either from the front (dark blue) or the back side (red) of the perovskite film.

To probe the optoelectronic properties of each region, we illuminated the films either from the front or the back side with 3.1 eV light and measured the PL spectra in reflection mode

1
2
3 (Figure 1.c). At this excitation energy, light is strongly absorbed by the lead iodide perovskite,
4
5 with an associated penetration depth shorter than 100 nm (See Figure S2) which means that the
6
7 initially generated charge-carrier distributions will be located either in the 3D MAPbI₃ or the
8
9 quasi-2D layers. We find that, as expected, front side photoexcitation produces a symmetric
10
11 narrow-band emission consistent with conventional 3D MAPbI₃ spectra,²⁷ while photoexcitation
12
13 on the back (substrate side) of the film, however, results in a higher energy shoulder in the
14
15 emission, in agreement with the presence of quasi-2D perovskite domains.
16
17
18
19
20
21
22

23 To further investigate how the charge-carrier distribution evolves through the film, we
24
25 measured the PL dynamics following photoexcitation from either the front (Figure 2.a,b) or back
26
27 side of the film (Figure 2.d,e). We find that when the film is excited from the back side, the PL
28
29 spectrum at early times carries the fingerprint of the quasi-2D region, which decays with a
30
31 lifetime of only 4 ns. This broad-band emission spectrum is superimposed onto the long-lived,
32
33 narrower emission spectrum of the 3D MAPbI₃ region, with lifetime > 1 μ s (see Figure S4 for
34
35 component analysis). We note that the high-energy emission of the quasi-2D region is centered
36
37 around 1.74 eV, in contrast to that reported for strongly confined 2D perovskites ($n=1$) of similar
38
39 composition which have exhibited emission in the 2.2 – 2.5 eV spectral region.²⁸ In addition,
40
41 there is no strong presence of sharp higher-energy bandgap phases in the absorption spectrum of
42
43 the film (Figure 1.c, dashed blue line). Although the broad PL emission observed from the
44
45 present samples does not allow for accurate determination of the n composition, it suggests a
46
47 predominance of $n>4$ quasi-2D domains. The exciton binding energies for such level of
48
49 dielectric and electronic confinement are not expected to be so significantly elevated as to be
50
51 detrimental for photovoltaic applications.^{29,30} Nonetheless, even such a low level of confinement
52
53
54
55
56
57
58
59
60

1
2
3 apparently has a dramatic effect on the radiative recombination rates of charge-carriers, as
4
5 evidenced by the high relative intensity and fast decay of the high energy emission originating
6
7 from the quasi-2D perovskite. Such high emission decay rates could potentially be a limiting
8
9 factor for photovoltaic devices, where long carrier lifetimes (i.e. long diffusion lengths) are
10
11 desirable to promote efficient charge extraction. However, these short lifetimes could
12
13 alternatively be associated with charge and energy transfer dynamics to the lower bandgap
14
15 domains, which would be beneficial, given that where these are likely to exhibit higher charge-
16
17 carrier lifetimes and mobilities, and lower exciton binding energies.
18
19
20
21
22
23
24
25
26
27
28
29
30
31
32
33
34
35
36
37
38
39
40
41
42
43
44
45
46
47
48
49
50
51
52
53
54
55
56
57
58
59
60

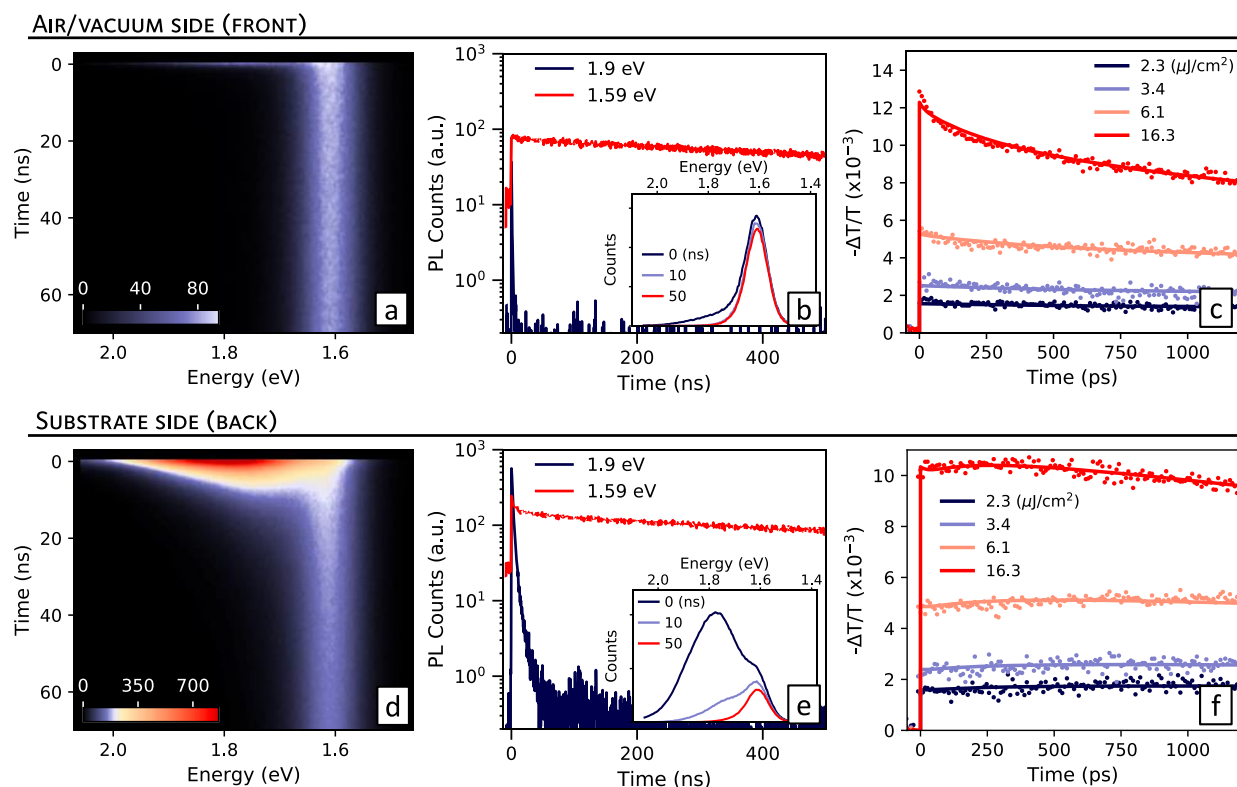


Figure 2. Maps of the time-resolved PL originating from a 3D/quasi-2D lead iodide perovskite film measured in reflection geometry, with photoexcitation from the front (a) or the back (d) of the films, taken with an excitation energy of 3.1 eV (500 kHz, fluence ~ 10 nJ/cm²); PL decays (point spacing ~ 3 ns) at 1.59 eV (red) and 1.9 eV (dark blue) taken with photoexcitation from the front (b) or the back (e) of the films; insets show the matching PL spectra at different decay times. OOTP THz photoconductivity transients (plotted as $-\Delta T/T \propto \sigma$; time resolution ~ 50 fs, excitation at 3.1 eV, repetition rate 5 kHz) taken with photoexcitation incident on the front (c) or back (f) of the films; dots are experimental data points and solid lines are fitted dynamics (which account for charge diffusion and photon reabsorption, and assume heterogeneous PL emission).

1
2
3 To investigate such interplay between confinement effects and the charge transport
4 properties of the mixed-phase films we performed OPTP spectroscopy, which allows us to probe
5 the transient photoconductivity of the film in a contactless manner. The measurements were
6 performed with 3.1 eV pulsed photoexcitation incident either on the front or back of the films,
7 and the transients obtained are shown in Figure 2.c,f. The photoinduced differential transmission
8 of THz radiation ($\Delta T/T$) is proportional to the photoconductivity (σ) of the film, which is in turn
9 linearly dependent on the charge-carrier population density and the effective charge-carrier
10 mobility (μ). From the $-\Delta T/T$ amplitude immediately after photoexcitation (i.e. before charge-
11 carrier recombination has occurred) μ can then be extracted under knowledge of the absorbed
12 photon density (see Section 1.5 in SI for details).^{31,32} We find that while photoexcitation from the
13 back side of the film resulted in an initial charge-carrier mobility 17.4 ± 0.9 cm²/Vs, this value
14 increased to 23.9 ± 0.9 cm²/Vs for excitation from the front side. The $\sim 25\%$ lower charge-carrier
15 mobility measured when probing the back side of the films is consistent with the presence of
16 quasi-2D domains and the higher concentration of dielectric barriers in this region.⁷
17
18
19
20
21
22
23
24
25
26
27
28
29
30
31
32
33
34
35
36
37
38

39 The OPTP measurements further allow us to investigate the subsequent dynamics of
40 charge-carriers following the initial photoexcitation. We note that unlike the PL transients
41 discussed earlier, which tend to overemphasize the contributions from carrier recombination in
42 strongly confined regions that are associated with high radiative efficiencies, the OPTP
43 photoconductivity measurements are particularly sensitive to carriers that are mobile, thus
44 highlighting the electronic response from regions of lower confinement. Figure 2.c,f shows that
45 both for back and front side photoexcitation the photoconductivity lifetimes decrease with
46 increasing fluence (for full fluence dependence see Figure S5 in the SI). This behavior can be
47
48
49
50
51
52
53
54
55
56
57
58
59
60

1
2
3 described by the typical recombination dynamics of free charge-carriers observed in perovskite
4
5 semiconductors, which may recombine through a monomolecular trap-assisted mechanism,
6
7 combined with bimolecular radiative recombination and third order Auger-like processes whose
8
9 contribution become significant at higher carrier densities.^{31,33} At the lowest fluences, transients
10
11 are generally expected to be flat, as bi-molecular and Auger recombination become negligible,
12
13 and the remaining trap-mediated recombination may occur over a time scale much longer than
14
15 the observation window of 1 ns. However, while the low-fluence dynamics for front-side
16
17 excitation of the film indeed appear mostly flat, the transients taken after photoexcitation of the
18
19 back side of the film show a rise in photoconductivity (Figure 3.a). Due to the short penetration
20
21 depth (<100 nm) of the excitation light, the $\Delta T/T$ signal immediately after photoexcitation arises
22
23 exclusively from the volume of the thin films in which light is absorbed and where the charge-
24
25 carriers are initially concentrated. The THz probe beam on the other hand has a penetration depth
26
27 much longer than the sample thickness and is detected in transmission geometry, therefore
28
29 responding to mobile charge-carriers present anywhere within the full volume of the film. In
30
31 consideration of the lower charge-carrier mobilities we have observed in the quasi-2D region of
32
33 the films, we can credit the rise in the OPTP dynamics following substrate-side photoexcitation
34
35 to the transfer of charge-carriers from the low-mobility quasi-2D region to the higher-mobility
36
37 3D region. By analyzing the resulting photoconductivity enhancement, we are thus able to
38
39 investigate the mechanisms underpinning such rapid transfer of charge-carriers.
40
41
42
43
44
45
46
47
48
49

50 Figure 3.b schematically illustrates the mechanisms by which charge-carriers may be
51
52 transferred from quasi-2D to 3D domains in the film. Here, we do not account for the transfer of
53
54 excitons but rather focus on the movement of free charge-carriers. Although exciton transfer has
55
56
57
58
59
60

1
2
3 been observed in layered perovskites,²⁶ it has been found to dominate at much shorter timescales
4
5 (~100 fs) and distances than we explore here, and in the presence of higher exciton binding
6
7 energies in strongly confined 2D layers, which are not present in our samples. We therefore
8
9 focus on two main transfer mechanisms, which are diffusion of free charge-carriers and photon
10
11 recycling.
12
13

14
15
16
17
18 The diffusion of free charge-carriers from the quasi-2D to the 3D domains will be aided
19
20 by the slight downward slope in bandgap energy (Figure 3) and the strong gradient in charge-
21
22 carrier density resulting from the short penetration depth of the photoexcitation, which will cause
23
24 both electrons and holes to diffuse preferentially away from the illuminated area. As we discuss
25
26 further below, given the measured values for charge-carrier mobilities, such diffusion should
27
28 indeed occur within the nanosecond timescales of our observations. We note that because the
29
30 photoconductivity probed by OPTP represents a sum of the electron and hole contributions, we
31
32 cannot distinguish between the individual dynamics of electrons and holes. However, recent
33
34 Ultraviolet Photoelectron Spectroscopy (UPS)^{9,34} measurements of quasi-2D lead iodide
35
36 perovskites have revealed that the energetic positions of the valence band maxima (VBM) show
37
38 little variation with layer thickness n , while the conduction band minima (CBM) show more
39
40 pronounced steps, thus forming an energy cascade for electrons (see Figure 3). Therefore, while
41
42 such a gradient in CBM will promote the transfer of electrons to lower-bandgap 3D domains
43
44 towards the front side of our films, the alignment of the VBM should allow free movement of
45
46 holes into any direction. Such hole transfer to higher band-gap domains has indeed been
47
48 previously observed by transient absorption spectroscopy.^{26,35-37} This characteristic has important
49
50 implications for solar cells fabricated with mixed-phase quasi-2D perovskites, as it allows for
51
52
53
54
55
56
57
58
59
60

1
2
3 facile charge separation of electrons and holes towards opposite electrodes when a gradient of
4
5 2D effects through the depth profile is present.
6
7
8
9
10

11 The second effective mechanism for the transfer of charges that needs to be considered is
12 the reabsorption of photons that have been emitted following radiative charge-carrier
13 recombination. Such photon recycling is known to have significant effects on the excited state
14 dynamics over the nanosecond timescale of our measurements.³⁸ As we show below, this process
15 will be particularly efficient for the case of high-energy photons originating from the highly
16 emissive quasi-2D domains, which have strong energetic overlap with the absorption spectrum
17 of the lower-bandgap 3D perovskite.
18
19
20
21
22
23
24
25
26
27
28
29
30
31
32
33
34
35
36
37
38
39
40
41
42
43
44
45
46
47
48
49
50
51
52
53
54
55
56
57
58
59
60

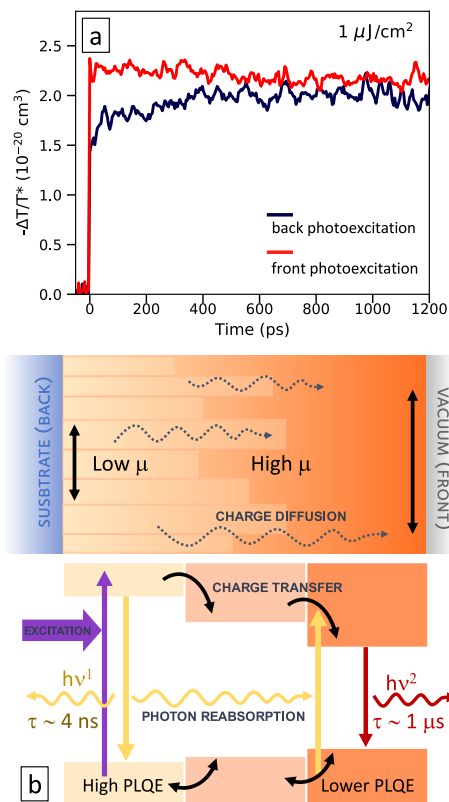


Figure 3. a) OPTP dynamics measured with illumination incident on the front (red) or back (dark blue) side of the thin film, with fluence $1 \mu\text{J}/\text{cm}^2$. In order to account for different photoexcitation densities that result from the different reflectivity of the perovskite (front) or substrate (back) surfaces, the amplitudes have been plotted as $-\Delta T/T^* = (-\Delta T/T)/N_0$, where N_0 is the predicted initial density of photoexcited carriers (see Figure S6 for unnormalized data). b) Schematic illustration of the charge-carrier transfer and recombination mechanisms operating in a thin metal halide perovskite film made of quasi-2D, higher bandgap domains near the substrate side, and a 3D, lower bandgap region near the front (vacuum) side.

1
2
3 To evaluate the relative importance of each of these mechanisms, we modelled the
4 photoconductivity dynamics based on a modified version of our previously reported approach,
5 that accurately described the observed OPTP dynamics in 3D perovskite films.³⁸ As before, we
6 account for the effects of the charge-carrier diffusion and photon reabsorption as well as carrier
7 recombination,³⁸ but in addition now also consider the heterogeneous distribution of morphology
8 and electronic properties through the film profile. Briefly, the initial charge-carrier population
9 after a short pulse of photoexcitation is determined according to Beer's Law of absorption, and
10 decays exponentially away from the illuminated surface. At any given depth of the film, the
11 carrier population evolves over time from its initial value, as a result of carrier recombination,
12 carrier diffusion and reabsorption of photons originating from radiative recombination that is
13 tracked through the film. The mixed-phase morphology of the films, with the presence of both
14 quasi-2D and 3D layers, requires us to account for the heterogeneous charge-carrier mobilities
15 and spectral shape of PL emission. Based on the experimental characterization of the film
16 detailed above, we modelled the mixed-phase films as comprising two layers: one on the
17 substrate side, consisting of a quasi-2D region of 150 nm thickness with effective mobility $\mu =$
18 17.4 cm²/Vs, on top of which resides a 3D perovskite layer with 300 nm thickness and $\mu = 23.9$
19 cm²/Vs (Figure S9). The characteristic PL emission spectra associated with each layer were
20 obtained from the PL spectra measured at early times after photoexcitation from either side (see
21 insets in Figures 2b,e), which were corrected to account for self-absorption effects (Figure S12).
22 A full description of the model is provided in Supporting Information.
23
24
25
26
27
28
29
30
31
32
33
34
35
36
37
38
39
40
41
42
43
44
45
46
47
48
49
50
51
52

53 Our model simulates the diffusion of charge-carriers based on the mobility and thickness
54 of each layer and traces the photon reabsorption according to the absorption and PL spectra and
55
56
57
58
59
60

1
2
3 the radiative rate. Simultaneously, the recombination rate constants are globally fitted to the
4
5 fluence dependence of the experimental transients. First, we are able to determine the intrinsic
6
7 value of the bimolecular recombination rate constant accurately from fits of the transients, shown
8
9 in Figure 2.c,f for both front and back photoexcitation and find a value similar to the one we
10
11 have recently reported⁸ for MAPbI₃ at room temperature (see Section S5 of the SI). Second, we
12
13 are able to concentrate on a careful examination of the photoconductivity transients collected at
14
15 lower excitation fluences, to investigate the relative importance of the individual contribution of
16
17 charge diffusion and photon reabsorption. Figure 4.b shows an example for such transients,
18
19 which exhibit a slow rise in photoconductivity for excitation from the back side (quasi-2D
20
21 region), but a decay for excitation from the front side (3D layer). In the former case, importantly,
22
23 initial excitation of the quasi-2D region leads to a crossing in the photoconductivity transient at
24
25 later times. This observation is surprising, given that for similar charge recombination rates, the
26
27 redistribution of charge-carriers would eventually result in a uniform population throughout the
28
29 film giving equivalent photoconductivity regardless of where carriers are initially photoexcited.
30
31 Alternatively, higher radiative losses in quasi-2D domains could ultimately result in lower
32
33 photoconductivity values. However, such crossing in the dynamics instead shows that the
34
35 photoconductivity attained at long times after excitation of the 2D phase exceeds that observed
36
37 for direct excitation of the 3D phase. To understand the origin of this enhancement of
38
39 photoconductivity, and the relative contributions of charge-carrier diffusion and photon
40
41 reabsorption, we applied the model to fit these transients with either or both of these mechanisms
42
43 omitted.
44
45
46
47
48
49
50
51
52
53
54
55
56
57
58
59
60

1
2
3 Focusing first on the differences in the OPTP transients observed at early times, we find
4 that exclusion of photon reabsorption from the dynamical model still allows us to reproduce the
5 dynamics with good accuracy (See Figures S13 and S14). Charge diffusion from quasi-2D
6 domains with lower carrier mobility to the high-mobility 3D region therefore appears to be the
7 main mechanism influencing the early transient enhancement of the photoconductivity following
8 excitation of the quasi-2D region. We observed that such a rise cannot be reproduced when only
9 photon reabsorption is used to redistribute carriers across the film. However, when considering
10 both mechanisms, reabsorption results in prolonged charge-carrier lifetimes and a further
11 enhancement of photoconductivity at later times, with respect to the effect of diffusion alone
12 (See Section S6.2 in Supporting Information).
13
14
15
16
17
18
19
20
21
22
23
24
25
26
27
28
29

30 Finally, we are able to relate the observed crossing of the transients (Figure 4.b) for front
31 and back excitation to the heterogeneous nature of the PL emission spectra in these films. We
32 observed that such crossing can only be reproduced when accounting for photon reabsorption.
33 We then evaluate how the sample heterogeneity affects the efficiency of photon recapture. Here,
34 we simulated the OPTP dynamics incorporating both charge diffusion and photon reabsorption,
35 but now consider two different spectral scenarios for photon reabsorption. In the first case, we
36 considered heterogeneous PL, where the emission of the quasi-2D region has two components
37 centered at 1.59 and 1.74 eV (as derived from back-surface excitation spectra) while the
38 emission of the 3D region is centered at 1.59 eV (as illustrated in Figure 4.a). In the second case,
39 we considered homogeneous PL across the film, that is, both regions exhibit emission centered at
40 1.59 eV (spectral shape of 3D MAPbI₃, as observed for front-surface excitation), and its overlap
41 with the absorption spectrum of the film that is dominated by 3D MAPbI₃ near the onset (Figure
42
43
44
45
46
47
48
49
50
51
52
53
54
55
56
57
58
59
60

1
2
3 1.c). As Figure 4.a illustrates, for the case of heterogeneous PL, the high energy photons emitted
4
5 by the quasi-2D domains overlap much better with the absorption coefficient spectrum of the 3D
6
7 domains, resulting in a 60% probability of photon recapture, compared with a 40% probability
8
9 for the case of 3D MAPbI₃ emission (see Section S6.2.1 in SI for full details of calculation). Such
10
11 improved spectral overlap between absorption and emission enables the quasi-2D PL emission to
12
13 contribute to a stronger enhancement of photoconductivity over time (Figure S21) as a
14
15 consequence of more efficient photon reabsorption by the 3D MAPbI₃ layer. As Figure 4.d
16
17 shows, the modelled OPTP transients for front photoexcitation (red) and back photoexcitation
18
19 (dark blue) will only cross at later times if heterogeneous PL is considered at this fluence, while
20
21 they approach each other at long times for the case of homogeneous PL. The experimentally
22
23 observed crossing of these transients (Figure 4.b) thus provides clear evidence that photon
24
25 reabsorption, boosted by the higher-energy emission of the quasi-2D region, augments capture
26
27 and retention of charge-carriers in the 3D perovskite layer.
28
29
30
31
32
33
34
35
36

37 Our modelling of photon reabsorption effects in these mixed-phase perovskite films thus
38
39 reveals two favorable effects. First, we find that photon recapture minimizes radiative losses,
40
41 even when charge-carriers recombine relatively rapidly in the quasi-2D phase of the material,
42
43 because of efficient photon recapture that prolongs the effective charge-carrier lifetime. As a
44
45 second effect, photon reabsorption leads to somewhat faster redistribution of charge-carriers
46
47 from quasi-2D to 3D domains then would be expected from charge diffusion alone. These two
48
49 effects are able to compensate, respectively, the increased charge-carrier recombination rate and
50
51 reduced mobility that characterize quasi-2D perovskites. Because radiative recombination is a
52
53 bimolecular process, photon reabsorption appears to affect the dynamics more strongly at higher
54
55
56
57
58
59
60

1
2
3 excitation fluences (Figure S7). At low excitation fluences, charge-carrier diffusion is the
4
5 dominant mechanism and the measured THz photoconductivity reaches the same amplitude for
6
7 both front and back excitation, because the charge-carrier density becomes evenly spread though
8
9 the film which compensates for the differences in charge mobilities between regions of the film.
10
11 At higher fluences, on the other hand, the contribution of radiative recombination increases,
12
13 making photon reabsorption particularly effective. Therefore, at the radiative limit, the more
14
15 highly optimized photon reabsorption resulting from better spectral overlap between the quasi-
16
17 2D emission and the 3D perovskite absorption ultimately results in slightly longer charge-carrier
18
19 lifetimes and increased photoconductivity when the quasi-2D side is illuminated. We also note
20
21 that the efficiency of photon recapture is not greatly affected by the total thickness of the film,
22
23 for values typically implemented in perovskite solar cells (see Section 6.3 in the SI). This boost
24
25 in lifetime and photoconductivity promoted by the higher PL energy of the quasi-2D phase
26
27 suggests that light-harvesting devices fabricated with such mixed-phase perovskite films could
28
29 benefit from illumination being incident on the side containing the quasi-2D material. In
30
31 addition, we note that the presence of quasi-2D domains should contribute to a decrease of non-
32
33 radiative losses. The passivation of grain boundaries by the large organic cation can decrease the
34
35 trap-assisted recombination rates, while the high radiative rates in the quasi-2D domains result in
36
37 higher PL quantum efficiencies.⁷⁹ Therefore, the heterogeneous photon recycling we observe here
38
39 will be particularly effective.
40
41
42
43
44
45
46
47
48
49
50
51
52
53
54
55
56
57
58
59
60

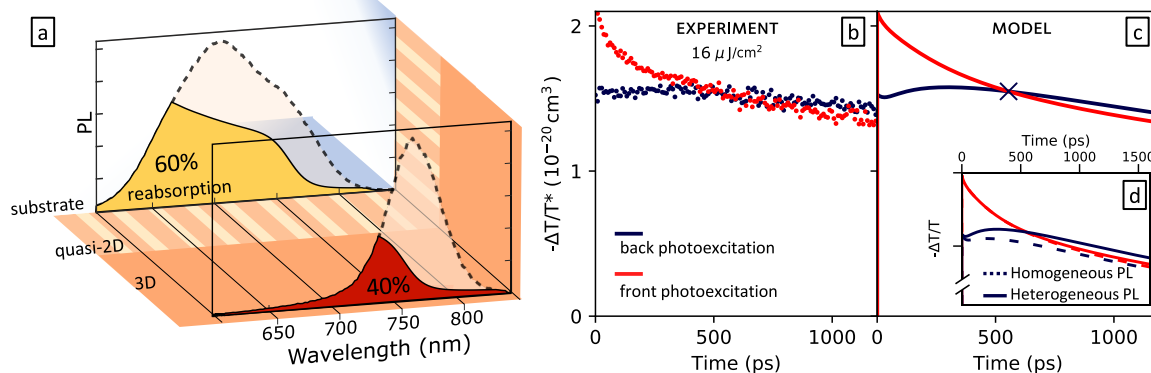


Figure 4. a) PL spectra (dashed line, corrected for self-absorption) of the quasi-2D and 3D lead iodide perovskite regions of the thin film. The highlighted area indicates the spectral overlap with the absorption spectrum. The calculated photon recapture probabilities are 40% for 3D emission and 60% for quasi-2D emission. b) OPTP dynamics measured with illumination incident on the front (red) or back (dark blue) side of the thin film, with fluence $16 \mu\text{J}/\text{cm}^2$. Dots represent experimental data and solid lines in (c) are simulated transients (accounting for charge diffusion and photon reabsorption under the assumption of heterogeneous PL emission; recombination rate constants were obtained from the fits to experimental data). d) Simulated OPTP photoconductivity dynamics for photoexcitation incident on the front (red) or back (dark blue) of the thin film, both accounting for charge diffusion and photon reabsorption, but considering either homogeneous (dotted lines) or heterogeneous (solid lines) PL emission. In order to account for different photoexcitation densities that result from the different reflectivity of the perovskite (front) or substrate (back) surfaces, the amplitudes have been plotted as $-\Delta T/T^* = (-\Delta T/T)/N_0$, where N_0 is the predicted initial density of photoexcited carriers (see Figure S8 for unnormalized data). Simulated transients in (c) and (d) were obtained for a fixed value of N_0 on both sides (see Section S6 in Supporting Information for full details of the analysis).

1
2
3
4
5
6
7
8
9
10 In conclusion, we have investigated the charge-carrier transport in lead iodide perovskite
11 films with a self-assembled graded structure comprising quasi-2D domains on the substrate side,
12 topped with a layer of 3D MAPbI₃. We find that, as expected, the presence of electronic
13 confinement results in lower charge-carrier mobility and significantly higher radiative
14 recombination rates. However, through analysis of the photoconductivity dynamics following
15 photoexcitation, we show why these effects still present no obstacle to the implementation of
16 these materials in photovoltaic cells. First, the rapid diffusion of charge-carriers to 3D perovskite
17 domains with higher charge-carrier mobility leads to a strong recovery of photoconductivity in
18 the semiconductor even after initial illumination of mostly the quasi-2D material. Second, the
19 efficient reabsorption of photons originating from charge-carrier recombination inside the quasi-
20 2D domains leads to a further boost in photoconductivity associated with prolonged charge-
21 carrier lifetimes. Such heterogeneous photon recycling is particularly effective because the
22 emission spectrum of the quasi-2D domains is blue-shifted beyond the absorption onset of the
23 3D perovskite. Thus, the effects of charge diffusion and photon recycling are able to compensate
24 for the less favorable aspects of dielectric confinement, for the graded structures under
25 investigation here. Such morphologies may therefore offer the best of both worlds, combining
26 enhanced moisture resistance and surface passivation through the incorporation of the large
27 hydrophobic cations, with excellent charge transporting properties needed for highly efficient
28 solar cells.
29
30
31
32
33
34
35
36
37
38
39
40
41
42
43
44
45
46
47
48
49
50
51
52
53
54
55
56
57
58
59
60

Supporting Information

Supporting Information available: Material preparation; structural and optical characterization data; experimental details of OPTP and PL setups, description of charge-carrier dynamics model; analysis of the effects of charge-carrier diffusion, photon reabsorption and quasi-2D layer thickness on OPTP transients.

References

- (1) NREL. Best Research-Cell Efficiencies <https://www.nrel.gov/pv/assets/images/efficiency-chart.png> (accessed May 23, 2018).
- (2) Yang, J.; Siempelkamp, B. D.; Liu, D.; Kelly, T. L. *ACS Nano* **2015**, *9* (2), 1955–1963.
- (3) Huang, J.; Tan, S.; Lund, P.; Zhou, H. *Energy Environ. Sci.* **2017**, *10* (11), 2284–2311.
- (4) Christians, J. A.; Miranda Herrera, P. A.; Kamat, P. V. *J. Am. Chem. Soc.* **2015**, *137* (4), 1530–1538.
- (5) Smith, I. C.; Hoke, E. T.; Solis-Ibarra, D.; McGehee, M. D.; Karunadasa, H. I. *Angew. Chemie Int. Ed.* **2014**, *53* (42), 11232–11235.
- (6) Yang, R.; Li, R.; Cao, Y.; Wei, Y.; Miao, Y.; Tan, W. L.; Jiao, X.; Chen, H.; Zhang, L.; Chen, Q.; et al. *Adv. Mater.* **2018**, 1804771.
- (7) Milot, R. L.; Sutton, R. J.; Eperon, G. E.; Haghighirad, A. A.; Martinez Hardigree, J.; Miranda, L.; Snaith, H. J.; Johnston, M. B.; Herz, L. M. *Nano Lett.* **2016**, *16* (11), 7001–7007.
- (8) Even, J.; Pedesseau, L.; Katan, C. **2014**, 3733–3741.
- (9) Yuan, M.; Quan, L. N.; Comin, R.; Walters, G.; Sabatini, R.; Voznyy, O.; Hoogland, S.; Zhao, Y.; Beauregard, E. M.; Kanjanaboos, P.; et al. *Nat. Nanotechnol.* **2016**, *11* (10), 872–877.
- (10) Sun, Y.; Zhang, L.; Wang, N.; Zhang, S.; Cao, Y.; Miao, Y.; Xu, M.; Zhang, H.; Li, H.;

- 1
2
3 Yi, C.; et al. *npj Flex. Electron.* **2018**, *2* (1), 12.
4
5
6 (11) Wang, N.; Cheng, L.; Ge, R.; Zhang, S.; Miao, Y.; Zou, W.; Yi, C.; Sun, Y.; Cao, Y.;
7
8 Yang, R.; et al. *Nat. Photonics* **2016**, *10* (11), 699–704.
9
10
11 (12) Chin, X. Y.; Perumal, A.; Bruno, A.; Yantara, N.; Veldhuis, S. A.; Martínez-Sarti, L.;
12
13 Chandran, B.; Chirvony, V.; Lo, A. S. Z.; So, J.; et al. *Energy Environ. Sci.* **2018**, *11* (7),
14
15 1770–1778.
16
17
18 (13) Zheng, H.; Liu, G.; Zhu, L.; Ye, J.; Zhang, X.; Alsaedi, A.; Hayat, T.; Pan, X.; Dai, S.
19
20
21 *Adv. Energy Mater.* **2018**, *8* (21), 1800051.
22
23
24 (14) Cao, D. H.; Stoumpos, C. C.; Farha, O. K.; Hupp, J. T.; Kanatzidis, M. G. *J. Am. Chem.*
25
26 *Soc.* **2015**, *137* (24), 7843–7850.
27
28
29 (15) Tsai, H.; Nie, W.; Blancon, J. C.; Stoumpos, C. C.; Asadpour, R.; Harutyunyan, B.;
30
31 Neukirch, A. J.; Verduzco, R.; Crochet, J. J.; Tretiak, S.; et al. *Nature* **2016**, *536* (7616),
32
33 312–317.
34
35
36 (16) Zhang, X.; Ren, X.; Liu, B.; Munir, R.; Zhu, X.; Yang, D.; Li, J.; Liu, Y.; Smilgies, D. M.;
37
38 Li, R.; et al. *Energy Environ. Sci.* **2017**, *10* (10), 2095–2102.
39
40
41 (17) Zhou, N.; Shen, Y.; Li, L.; Tan, S.; Liu, N.; Zheng, G.; Chen, Q.; Zhou, H. *J. Am. Chem.*
42
43 *Soc.* **2018**, *140* (1), 459–465.
44
45
46 (18) Tsai, H.; Asadpour, R.; Blancon, J. C.; Stoumpos, C. C.; Even, J.; Ajayan, P. M.;
47
48 Kanatzidis, M. G.; Alam, M. A.; Mohite, A. D.; Nie, W. *Nat. Commun.* **2018**, *9* (1), 2130.
49
50
51 (19) Wang, Z.; Lin, Q.; Chmiel, F. P.; Sakai, N.; Herz, L. M.; Snaith, H. J. *Nat. Energy* **2017**, *2*
52
53 (9), 17135.
54
55
56
57
58
59
60

- 1
2
3 (20) Quan, L. N.; Yuan, M.; Comin, R.; Voznyy, O.; Beauregard, E. M.; Hoogland, S.; Buin,
4 A.; Kirmani, A. R.; Zhao, K.; Amassian, A.; et al. *J. Am. Chem. Soc.* **2016**, *138* (8), 2649–
5 2655.
6
7
8
9
10 (21) Straus, D. B.; Hurtado Parra, S.; Iotov, N.; Gebhardt, J.; Rappe, A. M.; Subotnik, J. E.;
11 Kikkawa, J. M.; Kagan, C. R. *J. Am. Chem. Soc.* **2016**, *138* (42), 13798–13801.
12
13
14
15 (22) Neutzner, S.; Thouin, F.; Cortecchia, D.; Petrozza, A.; Silva, C.; Srimath Kandada, A. R.
16 *Phys. Rev. Mater.* **2018**, *2* (6), 064605.
17
18
19
20 (23) Thouin, F.; Valverde-Chávez, D. A.; Quarti, C.; Cortecchia, D.; Bargigia, I.; Beljonne, D.;
21 Petrozza, A.; Silva, C.; Srimath Kandada, A. R. *Nat. Mater.* **2019**, *18* (4), 349–356.
22
23
24
25 (24) Liu, J.; Leng, J.; Wu, K.; Zhang, J.; Jin, S. *J. Am. Chem. Soc.* **2017**, *139* (4), 1432–1435.
26
27
28
29 (25) Chen, P.; Meng, Y.; Ahmadi, M.; Peng, Q.; Gao, C.; Xu, L.; Shao, M.; Xiong, Z.; Hu, B.
30 *Nano Energy* **2018**, *50*, 615–622.
31
32
33
34 (26) Proppe, A. H.; Elkins, M. H.; Voznyy, O.; Pensack, R. D.; Zapata, F.; Besteiro, L. V.;
35 Quan, L. N.; Quintero-Bermudez, R.; Todorovic, P.; Kelley, S. O.; et al. *J. Phys. Chem.*
36 *Lett.* **2019**, 419–426.
37
38
39
40 (27) Wehrenfennig, C.; Liu, M.; Snaith, H. J.; Johnston, M. B.; Herz, L. M. *J. Phys. Chem.*
41 *Lett.* **2014**, *5* (8), 1300–1306.
42
43
44
45 (28) Mao, L.; Tsai, H.; Nie, W.; Ma, L.; Im, J.; Stoumpos, C. C.; Malliakas, C. D.; Hao, F.;
46 Wasielewski, M. R.; Mohite, A. D.; et al. *Chem. Mater.* **2016**, *28* (21), 7781–7792.
47
48
49
50 (29) Blancon, J. C.; Tsai, H.; Nie, W.; Stoumpos, C. C.; Pedesseau, L.; Katan, C.; Kepenekian,
51 M.; Soe, C. M. M.; Appavoo, K.; Sfeir, M. Y.; et al. *Science (80-.)*. **2017**, *355* (6331),
52
53
54
55
56
57
58
59
60

- 1
2
3 1288–1292.
4
5
6 (30) Tsai, H.; Nie, W.; Blancon, J. C.; Stoumpos, C. C.; Asadpour, R.; Harutyunyan, B.;
7
8 Neukirch, A. J.; Verduzco, R.; Crochet, J. J.; Tretiak, S.; et al. *Nature* **2016**, *536* (7616),
9
10 312–317.
11
12
13 (31) Wehrenfennig, C.; Eperon, G. E.; Johnston, M. B.; Snaith, H. J.; Herz, L. M. *Adv. Mater.*
14
15 **2014**, *26* (10), 1584–1589.
16
17
18 (32) Herz, L. M. *ACS Energy Lett.* **2017**, *2* (7), 1539–1548.
19
20
21
22 (33) Johnston, M. B.; Herz, L. M. *Acc. Chem. Res.* **2016**, *49* (1), 146–154.
23
24
25 (34) Cao, D. H.; Stoumpos, C. C.; Farha, O. K.; Hupp, J. T.; Kanatzidis, M. G. *J. Am. Chem.*
26
27 *Soc.* **2015**, *2*, 150528135055008.
28
29
30 (35) Liu, J.; Leng, J.; Wu, K.; Zhang, J.; Jin, S. *J. Am. Chem. Soc.* **2017**, *139* (4), 1432–1435.
31
32
33 (36) Shang, Q.; Wang, Y.; Zhong, Y.; Mi, Y.; Qin, L.; Zhao, Y.; Qiu, X.; Liu, X.; Zhang, Q. *J.*
34
35 *Phys. Chem. Lett.* **2017**, *8* (18), 4431–4438.
36
37
38 (37) Proppe, A. H.; Quintero-Bermudez, R.; Tan, H.; Voznyy, O.; Kelley, S. O.; Sargent, E. H.
39
40 *J. Am. Chem. Soc.* **2018**, *140* (8), 2890–2896.
41
42
43 (38) Crothers, T. W.; Milot, R. L.; Patel, J. B.; Parrott, E. S.; Schlipf, J.; Müller-Buschbaum,
44
45 P.; Johnston, M. B.; Herz, L. M. *Nano Lett.* **2017**, *17* (9), 5782–5789.
46
47
48
49
50
51
52
53
54
55
56
57
58
59
60